Journal of Civil Structural Health Monitoring (2020) 10:43–56
https://doi.org/10.1007/s13349-019-00368-1

ORIGINAL PAPER

Static and dynamic testing of highway bridges: a best practice example

Marcheggiani Laura[1] · **Clementi Francesco**[2] · **Formisano Antonio**[3]

Received: 4 September 2019 / Accepted: 25 November 2019 / Published online: 2 December 2019

Abstract
The load bearing capacity of a viaduct and its structural behaviour under traffic or seismic excitation can be evaluated using well-established modelling methods aided by computing facilities of great capability. However, to ensure reliable results, numerical models used in designing should be calibrated with accurate information on material properties and structural components. The static and dynamic testing procedures applied to a multi-span bridge along a new highway link inaugurated in 2014 in northern Italy are examined as a best practice example. The structural responses and performances are compared with and evaluated in the light of static and dynamic load test results. In particular, Operational Modal Analysis and Experimental Modal Analysis are used and compared to match with the numerical model. The comparison showed that the dynamic load test can supplement the static load test for the structural evaluation of new viaducts; it may also be taken as an alternative for the monitoring of operational viaducts.

Keywords Structural health monitoring · Bridge · Load testing · Dynamic testing · Operational modal analysis · Experimental modal analysis

1 Introduction

Structural Health Monitoring (SHM) techniques have received considerable attention from academics and engineering practitioners in the last two decades, in different branches of the discipline. Monitoring the integrity of different systems and/or components is widely used, also in an automated manner, becoming common in automotive and aerospace engineering with several successful applications. Despite the theoretical and practical developments nowadays available, civil engineering is otherwise still reluctant to apply SHM techniques to a large scale. The reasons for this mistrust are various [1]: (i) the strong variety of structural types and situations involved in the construction industry; (ii) dramatic differences in terms of economic interests, size and technical skills of the subjects involved in the civil engineering sector, including facility owners, designers, and contractors; (iii) the absence of understanding of the potentiality of the SHM techniques.

Governments and professional groups related to civil engineering write and publish standard, guidelines, and simple recommendations to protect the safety of crucial infrastructures [2]. The developments observed in recent decades started with the Intelligent Sensing for Innovative Structures (ISIS) research network of Canada in 2001 [3], where a clear description of the SHM techniques is reported, obviously related to the knowledge in the time of writing, including static and dynamic tests. The US Federal Highway Administration (FHWA) and the International Federation for Structural Concrete (FIB) published guidelines for the development of an SHM model for monitoring bridges [4] as well as for monitoring and evaluating the safety of concrete bridges [5]. The International Organization for Standardization (ISO) proposed some years later new international standards [6] for measuring and processing the responses to vibrations of bridges. The EU guidelines of 2006 [7] present clear procedures and technologies for structural assessment, monitoring and control (SAMCO) of infrastructures. The

✉ Formisano Antonio
antoform@unina.it

[1] ENEA–Centro Ricerche Bologna e Laboratori di Ricerca Faenza, Bologna, Italy

[2] Department of Civil and Building Engineering, and Architecture (DICEA), Polytechnic University of Marche, Ancona, Italy

[3] Department of Structures for Engineering and Architecture, University of Naples Federico II, Naples, Italy

GOST R 53778:2010 [8] was published four years later, and in 2012, the German guidelines were added for the monitoring of bridges and other engineering [9].

In China, along with the rapid growth of its economics, a quick infrastructural deployment has been generated with the subsequent development of standard and regulation, also on SHM [10]. In Japan, together with the advancement of bridge SHM [11], new standards for the SHM design were added [12]. A wide selection of international codes is reported in [2]. In Italy, we notice a lack in SHM guidelines and procedures being simply limited to §9.2 of the Italian law [13], except for UNI 10985:2002 [14]. However, the Morandi Bridge disaster in Genoa (14 August 2018) and a long series of collapses and failures (22 October 2013, the Carasco Bridge, above the Sturla River, in the Genoese hinterland; 29 October 2016, overpass on the SS 36 in the province of Lecco; 9 March 2017, overpass 167 on the A14 motorway between Loreto and Ancona Sud; 18 April 2017, viaduct on the Fossano Cuneo ring road) demonstrate the need of reviewing the regulations and the urge for a national monitoring plan of the structural health of road infrastructures, for both new and existing ones. In specific, the Italian law gives the possibility to perform a static test and, if necessary, dynamic surveys (not compulsory).

Dynamic techniques play an important role from several points of view among the current tools for structural health monitoring. They mostly allow us to identify the main parameters governing the dynamic behavior of a bridge by measuring the structural response, namely natural frequencies, mode shapes, and damping factors, usually gained by means of Ambient Vibration Tests (AVTs) using operational identification methods. AVTs generally are less effective than Harmonically Forced Tests (HFTs), but their use does not require any additive equipment. Moreover, since they can be easily repeated, measurements of a high number of points are easily feasible even with a small number of available sensors [15–19]. In addition, recent advances on signal processing techniques applied to output-only measurements allow us to obtain accurate and reliable modal parameters' estimates.

Dynamic data collected during experiments are fundamental since they constitute a signature of the structural behavior of the bridge. However, these information become more effective and provide more significant results when used to improve a Finite Element Model (FEM) of the bridge, both for existing and new ones.

This paper reports, as a best practice example, the results of the testing procedure of one of the three main bridges along the new A35 BreBeMi motorway link between the cities of Brescia and Milan, in northern Italy, opened to traffic in July 2014. In particular, the main steps and results obtained on the bridge crossing the Adda river are analyzed. The most interesting aspect of the investigation consisted of the request of the Client to carry out both the environmental and the forced dynamic tests. The literature is rich in articles concerning dynamic tests performed on bridges, with assessments both in favor and against the AVT compared to the HFT. However, there are very few cases in which there was the possibility of performing both tests in a row, providing a detailed study by-passing each predetermination and evaluating not only qualitatively but also quantitatively the advantages and disadvantages of the two approaches.

2 The investigated bridge

The investigated viaduct, wbs VI003, extends between the Pk 43 + 220.95 and the Pk 44 + 487.92 with respect to the East–West motorway axis of the A35 Brebemi (Fig. 1); one of its main spans crosses the Adda river, which, therefore, gives it the name. The Adda Viaduct is composed of two side-by-side decks each made up of 20 spans with different lengths: shore spans of 45 m, typological spans 60 m, main spans of 90 m across the riverbed of the Adda river and the spillway of the Muzza canal, and transition spans of 75 m between the last ones and the typological ones. The deck is

Fig. 1 3D view of the Adda Viaduct

supported by piers with a full circular section with a height ranging from 4.70 m to 11.59 m. The two carriageways have an offset (along the longitudinal direction of the viaduct) of about 7 m, to allow the crossing of the river.

The plinths supporting the piers are circular-based foundations on the consolidated ground (Jet-Grouting) that can be grouped into four types, with a height between 2 and 2.5 m and a diameter between 8.70 and 12.50 m. The deck is joined to the side embankments by means of the abutments, as wide as the deck (i.e., 17.05 m) and having a height between (single elevation of the front wall) 8.55 m (shoulder S2 South roadway) and 7.99 m (shoulder S1 North roadway). In the viaduct, there are four artifacts with identical foundations and differentiated carpentry in the elevation of the ramp walls and in the shape of the gravel wall (which follows the transverse slope of the viaduct to the supports). The abutments on the same side are kept separated, despite the proximity of the artifacts, to decouple their behavior in a seismic scenario (Fig. 2). The plinths supporting the abutments are rectangular-based foundations on the consolidated ground (Jet-Grouting) having the same dimensions for all four abutments: $18.00 \times 14.00 \times 2.00$ m^3.

The decks are continuous beams made by the solidarization of individual "crutches" constituted with the prefabricated ashlar system with symmetrical cantilevered advance regarding the piers head. In particular, the continuous prefabricated box decks are assembled on site using the prestress technique with internal sliding cables.

From the seismic point of view, the viaduct belongs to the category of continuous deck bridges with seismic isolation. The usual apparatus supporting the deck on the support structures are replaced by seismic isolators with the aim of containing the seismic energy transmitted by the substructure (piles and abutments) to the superstructure (deck). The sliding pendulum isolators adopted incorporate good dissipating capabilities against the seismic action, guaranteeing very small residual displacements at the end of a possible seismic event. These devices are characterized by a distinctly nonlinear behavior, directly depending to the transmitted excitation. Within modest excitations, they assume pseudo-elastic behavior with stiffness characteristics related to the extent of the actions applied.

3 Static load test

To measure the deflections of the viaduct, loading and unloading sessions were carried out with different configurations of trucks, each one having a total weight of 420 kN. To get the maximum bending stresses, the trucks were arranged in the spans of 45 m and 60 m as in Fig. 3a, for the span of 75 m and 90 m as Fig. 3b, with the loads transversely centered [20].

The transverse position of the convoys close to the sights was studied to minimize the deformation of the lateral overhangs, so that the height of the tip of the overhang was really indicative of the average height of the cross section. The displacement in the middle of the span was read through two optical sights placed in correspondence of the lateral curbs, between the second and third rows of trucks.

To generate the design shear in a general pier (axis), a loading train was used with nine trucks arranged on three rows with a longitudinal center distance of 9.5 m (Fig. 4a). Finally, to generate the maximum torque, eight trucks are arranged, positioned in pairs close to the side overhang (Fig. 4b).

The measurement was based on the precision spirit leveling technique, with an accuracy of ± 0.01 mm. During the sessions, the deflections were measured at significant points identified as eleven benchmarks (see marker points in Figs. 3 and 4) fixed rigidly to the upper surface of the slab: given the geometry of the deck, the measurements were not

Fig. 2 A general layout of the Adda Viaduct

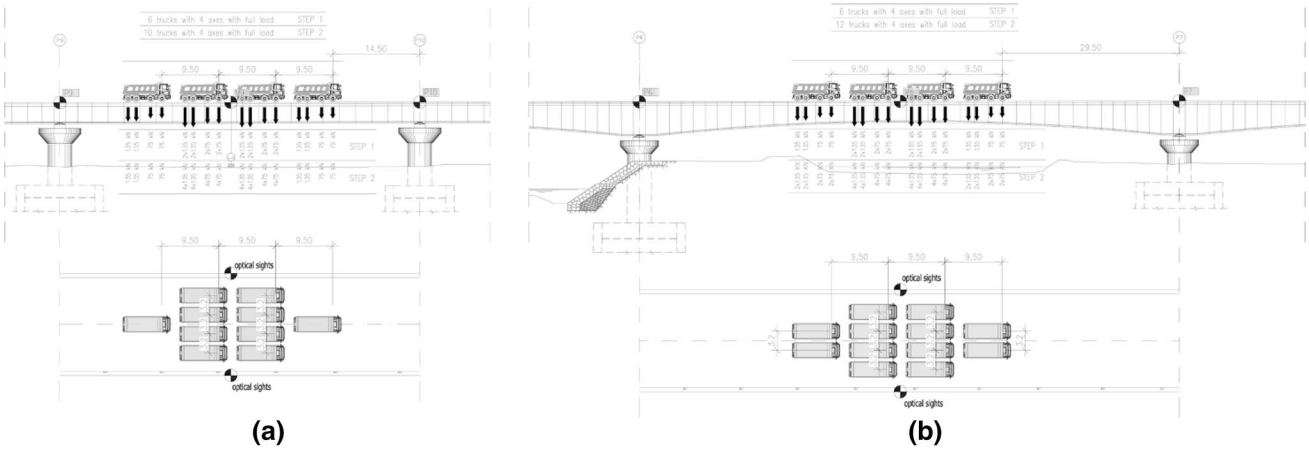

Fig. 3 A general scheme for the trucks during static load tests of the Adda Viaduct for the maximization of the bending in the span

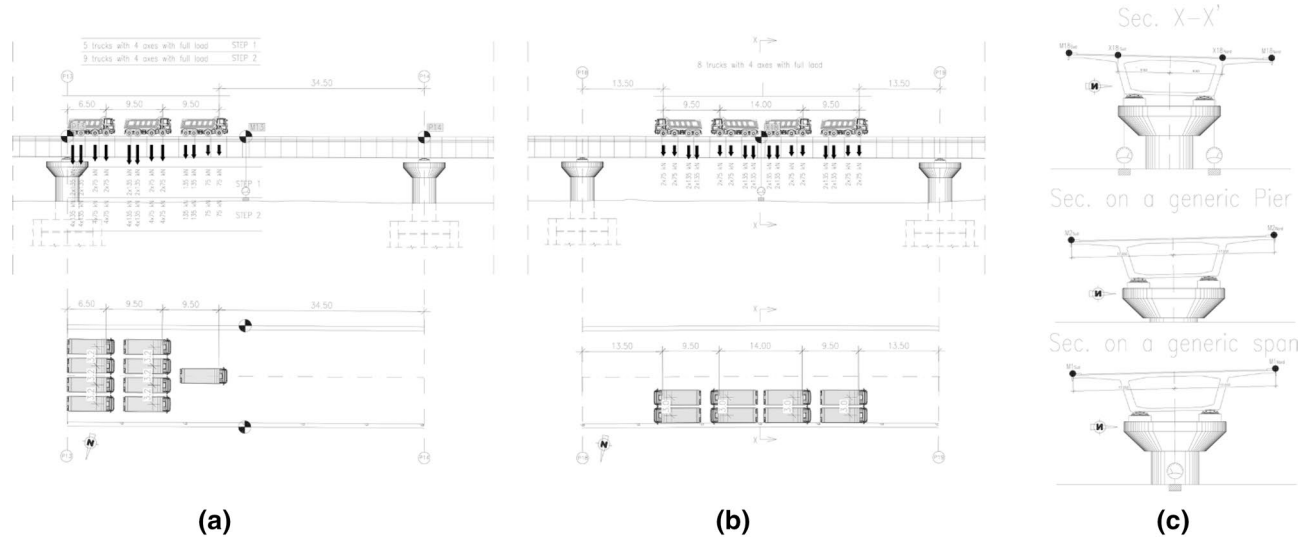

Fig. 4 A general scheme for the trucks during static load tests of the Adda Viaduct for the maximization of the shear in the piers and of the torsion in the deck

limited to the central span only, but to catch all the possible displacements, the optical sights were positioned in the external parts.

The measuring station consisted of a TRIMBLE 5603 robotic reflectorless total station, with 3″ of angular precision, reading accuracy at the leveling staff of 0.01 mm; with an automatic dual-axis compensator granting a working range of 6′, a magnification of 26×. The robotic station and the markers are reported in Fig. 5a. Measurements were carried out for each loading and unloading session by performing the readings on the staffs on the deck benchmarks and on an external benchmark (CS) positioned near the vertices of the station. To monitor the actual deformations induced by solar radiation, in order to remove the deformation of the deck under the load induced by this effect, optical targets were positioned also in correspondence of the parallel discharged roadway (the load test was carried out on the two carriageways at different times). Therefore, during the course of the load test, a monitoring of the discharge of the deck deformations was carried out, caused by solar radiation effects only. During the readings, the level was moved onto each of the three station vertices, thus allowing both collimations to the staff (even in the presence of the obstacles caused by the trucks) and redundancy of the measurements. The readings were not only digitally recorded but also transcribed in a field notebook.

Strain gauge transducers TLDT50MM, with a high-resolution measure of < 1 μm and a standard output of 2 mV/V, were used to limit possible measurement errors

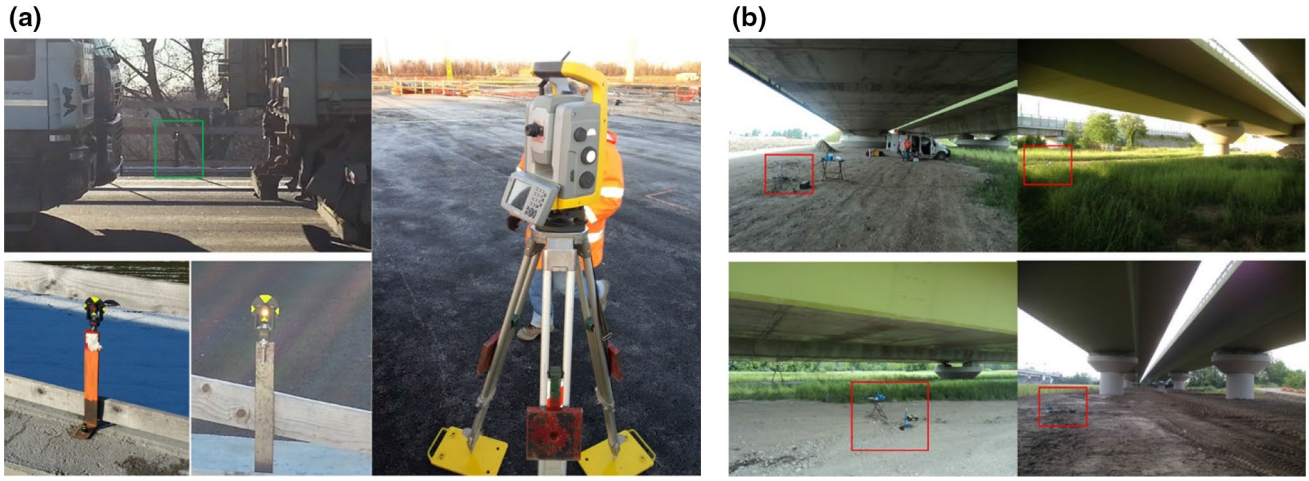

Fig. 5 The optical marker and the robotic reflectorless total station (**a**) and the LVDTs for the static load tests (**b**)

and correctly placed, to catch deflecting of bending and torsion (see Fig. 5b).

All the measurements were carried out in three different days. There were 16 load tests, each of them with both conditions of unloaded bridge (subject to its own weight alone) and loaded bridge (subject to the weight of different operational trucks): the trucks were placed—in a first step—in the decks to do an increment of loads of 60% for bending, 55% for shear, or directly 100% for torsion. The unloading conditions retraced the same steps until complete removal of the loads, and it stopped once the stabilization of the lowering residues was reached.

The measured and theoretical deflections for the bending action of the marker points (M_i for the middle of the beam, P_i for the piers) along the viaduct are reported in Table 1 for only the P6–P8 spans. The displacements of the directly loaded span are kept stable within the individual loading steps. The difference between the measured displacement to the net of the displacement of the supports (Δexp*) and the FEM displacement was always negative, so the structure behaved way better than expected during the design process. It is possible to state from the available data, not reported for brevity issue on this paper, that the displacement of the span preceding and following the loaded test is always acceptable, with a variation at least equal to -20% but always lower than the numerical one.

The exclusive measurement of the torsional deformation of the deck, expressed by the difference in the settlements under the load of the X18 south and X18 north sights (see Fig. 4), is reported in Table 2 for the span between the piers P18 and P19. Below the X18 sights, there are two centesimal fleximeters (F18 north and F18 south in Fig. 4) having a transverse distance of about 7.60 m. In this case, we have a good correlation with the optical measurements, with a variation of −4% that means a better behavior of the bridge with respect to the design exclamation. Comparing the results of the same points but with the LVDT, it is possible to observe an opposite behavior, worse than the numerical one, but always contained in an engineering-acceptable range.

In general, all the 16 tests showed an elastic behavior of the viaduct, with deformations related to the applied loads in the individual load steps and with negligible residual displacement (significantly less than 15% of the elastic deformation).

4 Dynamic load test

From 3 to 7 June 2014, AVT and HFT were carried out with the aim to assess the dynamic behaviors of the Adda Viaduct. In particular, span P5–P6, P6–P7, and P7–P8 (see Fig. 2) of the north carriageway and the spans at the lateral ends named S1–P1, P1–P2 and P2–P3 of the south carriageway were tested [21].

First of all, AVS was used to characterize the dynamic behavior of the bridge, with ambient vibration only, like wind, background noise, etc. The Operational Modal Analysis (OMA) technique was then used to obtain the main frequencies, the associated modal shapes, and the damping ratios.

Then, the HFT was used with a known and controlled input, and the correlated induced vibration was acquired, also providing a ratio between output and input. The quantities obtained to express the dynamic behavior of the structure, regardless of the type and extent of the input force, were in this case known and measured. The modal parameters, thus, obtained should allow a more reliable dynamic analysis of the structure with respect to the OMA, since with the forced test the energy supplied at each frequency is much greater, and in any case, it can be reproduced after

Table 1 Experimental and FEM results for the P6 to P8 spans at different stages of the load tests for bending action

Northern roadway											
Loading step 1 (55–60%)	Marker	M4	P5	M5	P6	M6	P7	M7	P8	M8	LVDT
	ΔFEM (mm)	−3.3	0	10.4	0	−22.7	0	8.7	0	−2	8.7
	ΔEXP (mm)	−2.8	0.05	8.36	−0.01	−21.62	−0.12	7.38	0.06	−1.45	7.4
	ΔEXP* (mm)	−2.83	0	8.34	0	−21.56	0	7.41	0	−1.48	–
Loading step 2 (100%)	ΔFEM (mm)	−6.5	0	20.8	0	−45.4	0	17.4	0	−3.9	17.4
	ΔEXP (mm)	−5.95	0.1	17.04	−0.26	−40.42	−0.17	12.73	−0.08	−3.11	11.33
	ΔEXP* (mm)	−6	0	17.12	0	−40.21	0	12.85	0	−3.07	–
	Variation (%)	−8%		−21%		−13%		−35%		-27%	−54%
Unloading step 1 (55–60%)	ΔFEM (mm)	−3.3	0	10.4	0	−22.7	0	8.7	0	−2	8.7
	ΔEXP (mm)	−2.8	0.05	8.36	−0.01	−21.62	-0.12	7.38	0.06	−1.45	7.4
	ΔEXP* (mm)	−2.83	0	8.34	0	−21.56	0	7.41	0	−1.48	–
Unloading	ΔResidual (mm)	−0.05	−0.15	0.06	−0.12	−0.3	−0.05	0.38	0.11	−0.1	1.04
Southern roadway											
Loading step 1 (55–60%)	Marker	M4	P5	M5	P6	M6	P7	M7	P8	M8	LVDT
	ΔFEM (mm)	−3.3	0	10.4	0	−22.7	0	8.7	0	−2	8.7
	ΔEXP (mm)	−3.26	0.05	8.87	−0.22	−20.65	0.01	6.43	−0.1	−1.33	6.1
	ΔEXP* (mm)	−3.28	0	8.95	0	−20.55	0	6.47	0	−1.28	–
Loading step 2 (100%)	ΔFEM (mm)	-6.5	0	20.8	0	−45.4	0	17.4	0	−3.9	17.4
	ΔEXP (mm)	−5.34	−0.15	14.65	0.35	−43.21	0.19	14.32	0.04	−2.86	13.06
	ΔEXP* (mm)	−5.27	0	14.55	0	−43.48	0	14.2	0	−2.88	–
	Variation (%)	−23%		−43%		−4%		−23%		−35%	−33%
Unloading step 1 (55–60%)	ΔFEM (mm)	−3.3	0	10.4	0	−22.7	0	8.7	0	−2	8.7
	ΔEXP (mm)	−3.36	0.05	8.8	0.2	−21.3	0.15	7.57	0.03	−1.75	6.84
	ΔEXP* (mm)	3.38	0	8.68	0	−21.48	0	7.49	0	−1.76	–
Unloading	ΔResidual (mm)	−0.11	0.05	0.55	0.25	−0.91	0.14	0.31	0.14	0.1	0.47

Table 2 Experimental and FEM results for the P18–P19 spans at different stages of the load tests for torsion action

Northern roadway			
Loading	MARKER	X18 south/north	F18 south/north
	ΔFEM (mm)	5.6	4.84
	ΔEXP (mm)	5.4	5.2
	Variation (%)	−4%	7%
Unloading	ΔFEM (mm)	0	0
	ΔEXP (mm)	0	−0.69
Southern roadway			
Loading	MARKER	X18 south/north	F18 south/north
	ΔFEM (mm)	5.6	4.84
	ΔEXP (mm)	5.4	5.54
	Variation (%)	−4%	13%
Unloading	ΔFEM (mm)	0	0
	ΔEXP (mm)	0	−0.18

many years. In the specific case, it was decided to place all the energy available on a single frequency at a time, using a stepped type forcing sine. This choice, despite requiring longer duration tests, allowed to have the best control over the forcing imposed on the structure. To provide excitation, imposed by inertia, a system for vertical forcing was used. Moreover, a hydraulic actuator loaded with appropriate masses is employed. The choice was conditioned by the possibility of implementing the best control strategy, in terms of both the amplitude of forcing and frequency.

4.1 Instrumental layout

The AV response of the bridge with OMA was measured at different spans (see Fig. 6a) and with different acquisitions. In particular, the AVs consider the spans between the piers P5 and P8 for the north carriageway, and between the abutment S1 and the pier P3 for the south carriageway.

The accelerometers were fixed in direct contact with the structural elements (Fig. 6a) and parallel/perpendicular to the main directions of the span, to get both horizontal and vertical modes. The positions chosen were at 1/3L, 1/2L, 2/3L of considered spans.

In general, two different types of highly sensitive accelerometers, measuring in two orthogonal directions, were placed (see Fig. 6a): the dots measure the vertical and arrows the horizontal directions. Other accelerometers were

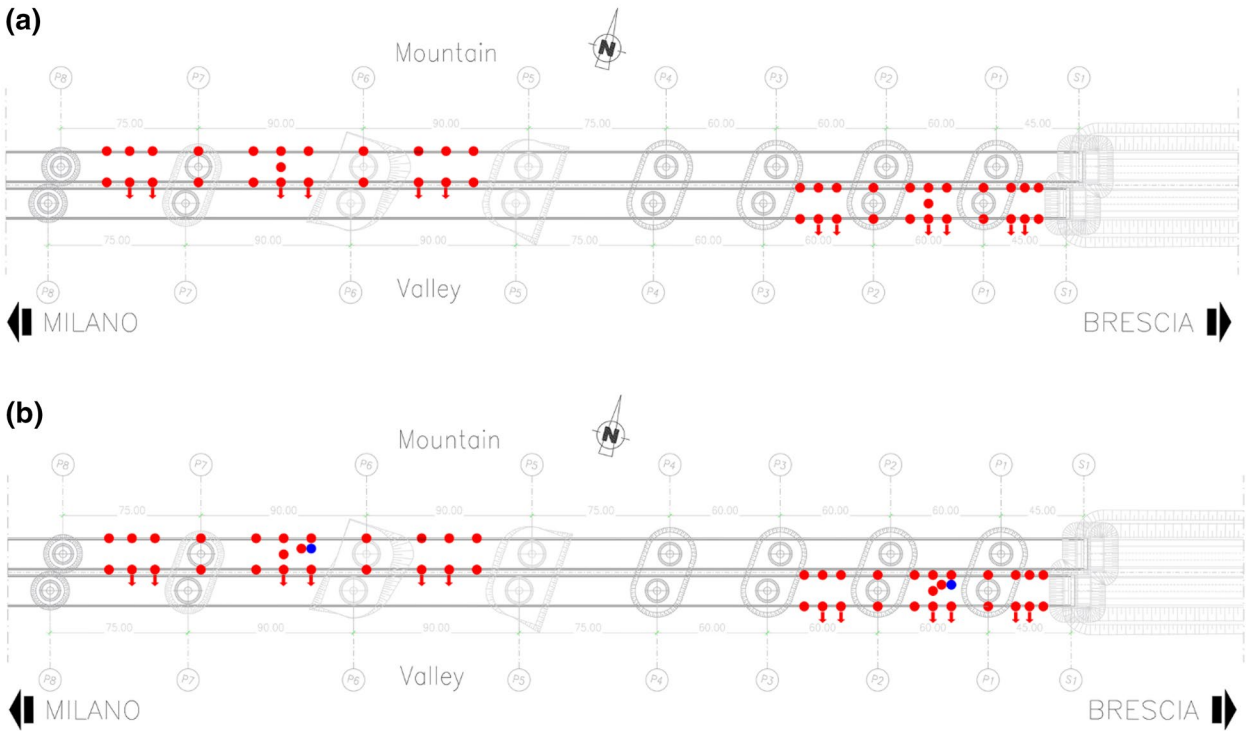

Fig. 6 Layout of the accelerometers at each span (see online version for colors) for operational modal analysis (**a**), and experimental modal analysis (**b**)

put in different positions as reported in Fig. 6a to obtain more information about the dynamic behavior of the whole structure.

A wired sensor network was used, composed of two types of piezoelectric sensors (Integrated Electronic Piezoelectric-IEPE):

393B12-PCB with voltage sensitivity of 10 V/g with a passband 0.15–1000 Hz, and measurement range of ± 0.5 g,

393B31-PCB with voltage sensitivity if 10 V/g with a passband 0.1–200 Hz, and measurement range of ± 0.5 g.

The digital recorder is composed of NI9234 modules with 24-bit A/D converter and integrated anti-aliasing filters. The data were acquired with a sampling frequency of 2048 Hz, pre-filtered and decimated 8 times, obtaining a final sampling frequency of 256 Hz.

For the Experimental Modal Analysis (EMA), the setup layout is essentially the same as OMA to facilitate comparison between the results of the two tests, but in this case, the excitation is provided by an inertial exciter (see blue point in Fig. 6b). The chosen position for the inertial exciter is close to 1/3L, where L is the length of the central span of the three measured portions, to excite the greatest number of eigenmodes at low frequency; the actuator has been placed in an asymmetrical position in reference to the center line, to force both vertical and torsional modes of the viaduct (at least in this part).

The hydraulic actuator (see Fig. 7) is powered by a portable pump with adequate characteristics. The actuator oscillates, at the desired frequency and amplitude, with its mass of 500 kg which generates the desired forcing on the structure. The chosen test profile is a stepped sine: within the frequency range of interest, a harmonic excitation at a fixed frequency is provided for a period sufficient to stabilize the behavior of the structure and to collect sufficient data for a complete and accurate analysis. The frequency is increased with variable steps, cooled around the structural resonances, with a minimum step of 0.01 Hz. The system has been specially designed and built to allow the best modulation of the load and the stroke, as the two variables, along with the frequency, influence the extent of forcing.

To estimate the force transmitted to the structure, an accelerometer (PCB 393A03 with a sensitivity of 1000 mV/g) was fixed to the basket that carried the mobile masses; starting from this measurement, since the moving mass is known, it was possible to detect the force value transmitted to the ground. The main values of the forces transmitted to the viaduct are reported in Table 3.

4.2 Operational modal analysis

Natural frequencies, vibrations modes and damping ratios were estimated for the lower modes of Girders North and

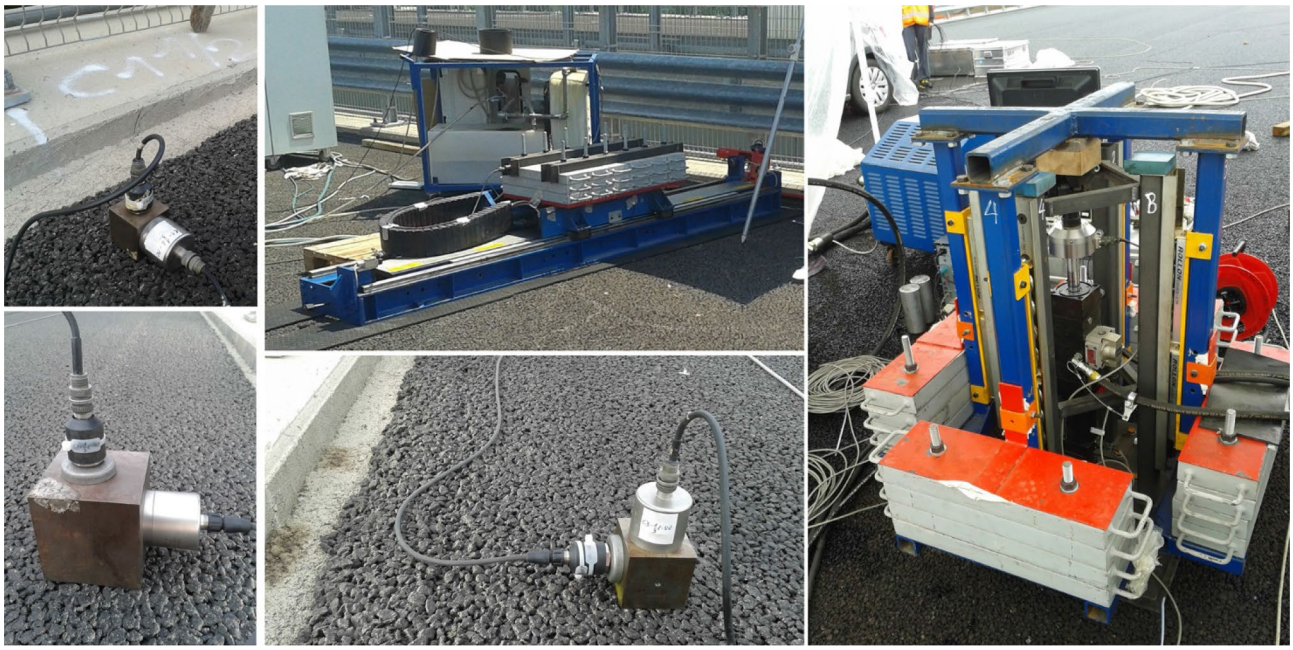

Fig. 7 Hydraulic actuator and accelerometers of the system for experimental modal analysis

Table 3 Forces transmitted on the deck for Experimental Modal Analysis for the two carriageways

Frequency (Hz)	North carriageway Force (N)	South carriageway Force (N)
1–1.5	800	800
1.5–1.8	1500	1000
1.8–2	1800	1500
2–2.5	2500	3000

South. The Time-Histories (THs) are analyzed by the Polyreference Least Square Frequency Domain [22].

Figure 8 shows the graph of the Power Spectral Density (PSD) of the accelerations detected during the 8 h of acquisition made on the North carriageway. Only three vibration modes were completely identified from the tests on North carriageway, see Fig. 9. The first and third modes involved a deformation of the bridge deck, with a prevalence of vertical oscillations, i.e., transversal to the deck. Mode 1 (1.27 Hz, $\zeta = 0.67\%$) corresponded to a bending in-phase deformation of the deck, i.e., the out-of-plane deformation of the deck was the same with equal sign at the extremities, as happened for the Mode 3 (1.68 Hz, $\zeta = 0.48\%$). In both cases, modal amplitudes changed of sign while crossing the piers for mountain extremity, and they always remain negative at the extremity of the valley, except at P6 where it assumed almost no value, therefore coinciding with the undeformed axis of the beam; vertical oscillations are dominant and the deck vibrates according to lower mode shapes of a multi-span continuous beam.

The Mode 2 (1.59 Hz, $\zeta = 0.79\%$) vibrates both in out-of-plane and in-plane directions of the deck. Maximum amplitudes were recorded in the first span if we consider the extremity near to the mountain, and in the middle of the central span, taking into account the extremity near to the valley, and the oscillation amplitudes of homologous points located on both sides of the deck were approximately equal but with opposite signs. These modes are reminiscent of the spatial deformation of the first bending modes of a multiple-span continuous beam.

A dynamic behavior analogous to that of North carriageway was encountered in identifying the vibration modes of South carriageway, with some little differences. Three frequencies and the associated mode shapes were identified also in this carriageway. The most important differences are that all the modes still involved the deformation of the whole deck, with a prevalence of an in-phase oscillation of the two extremities of the deck in the vertical plane. These modes had very close natural frequency values, respectively, 2.06 Hz and 2.11 Hz for Mode 1 and Mode 2. The third mode corresponded to the natural frequency value equal to 2.21 Hz and presented a modal deformation with a greater contribution in anti-phase at the stack closest to Milan.

As a consequence of these choices, it was noted from the examination of the results that the identification made on the North carriageway can identify with certainty the first three modes, while that on the South carriageway can identify only higher frequency modes (from 2.06 Hz forward), since

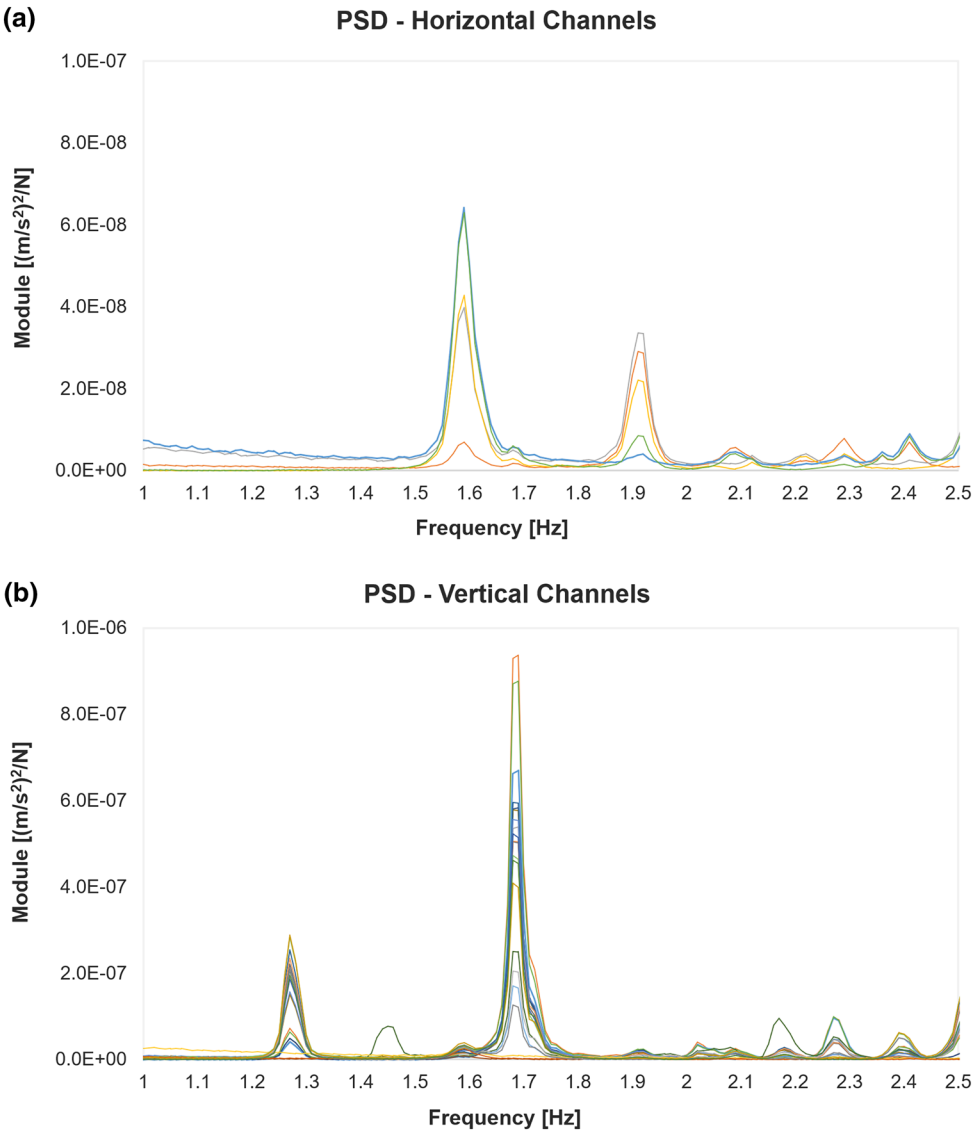

Fig. 8 PSD of horizontal (**a**) and vertical channels (**b**) for the OMA on the north carriageway [21]

the first three are locally producing modal deformations that are too low to be appreciated at the vibration levels which are typically found in the OMA. This is due to the fact that in the northern carriageway were tested the spans with the greatest span; in the South carriageway we tested those starting from the shoulder of the bridge. For brevity issues, this paper will not show PSD and mode shapes for the south carriageway.

4.3 Experimental modal analysis

On both carriageways, in addition to the AVTs, tests were carried out with known dynamic excitation, i.e., HFT, supplied by means of an oleodynamic exciter, according to the approach called EMA. All the available energy was applied on one frequency at a time, using a stepped sine forcing. The Time-Histories (THs) are analyzed by the Polyreference Least Square Frequency Domain [22].

Figure 10 shows the frequency response function (FRF) of the accelerations detected during acquisition on the North carriageway. The same first three vibration modes of OMA were completely identified, as seen in Fig. 11.

The first and third modes involved again a deformation of the bridge deck, with a prevalence of vertical oscillations, i.e., transversal to the deck. Mode 1 (1.26 Hz, $\zeta = 0.66\%$) corresponded to an out-of-plane deformation of the deck with the same sign in the extremities, with a difference in terms of frequencies respect to OMA of about $+0.79\%$. The same happened in Mode 3 (1.69 Hz, $\zeta = 0.63\%$) with a difference in terms of frequency of about -0.60% referred to OMA. For Mode 1, modal amplitudes changed sign crossing the piers; while for Mode 3, the modal amplitudes did not change signs in pier P6 remaining always negative in

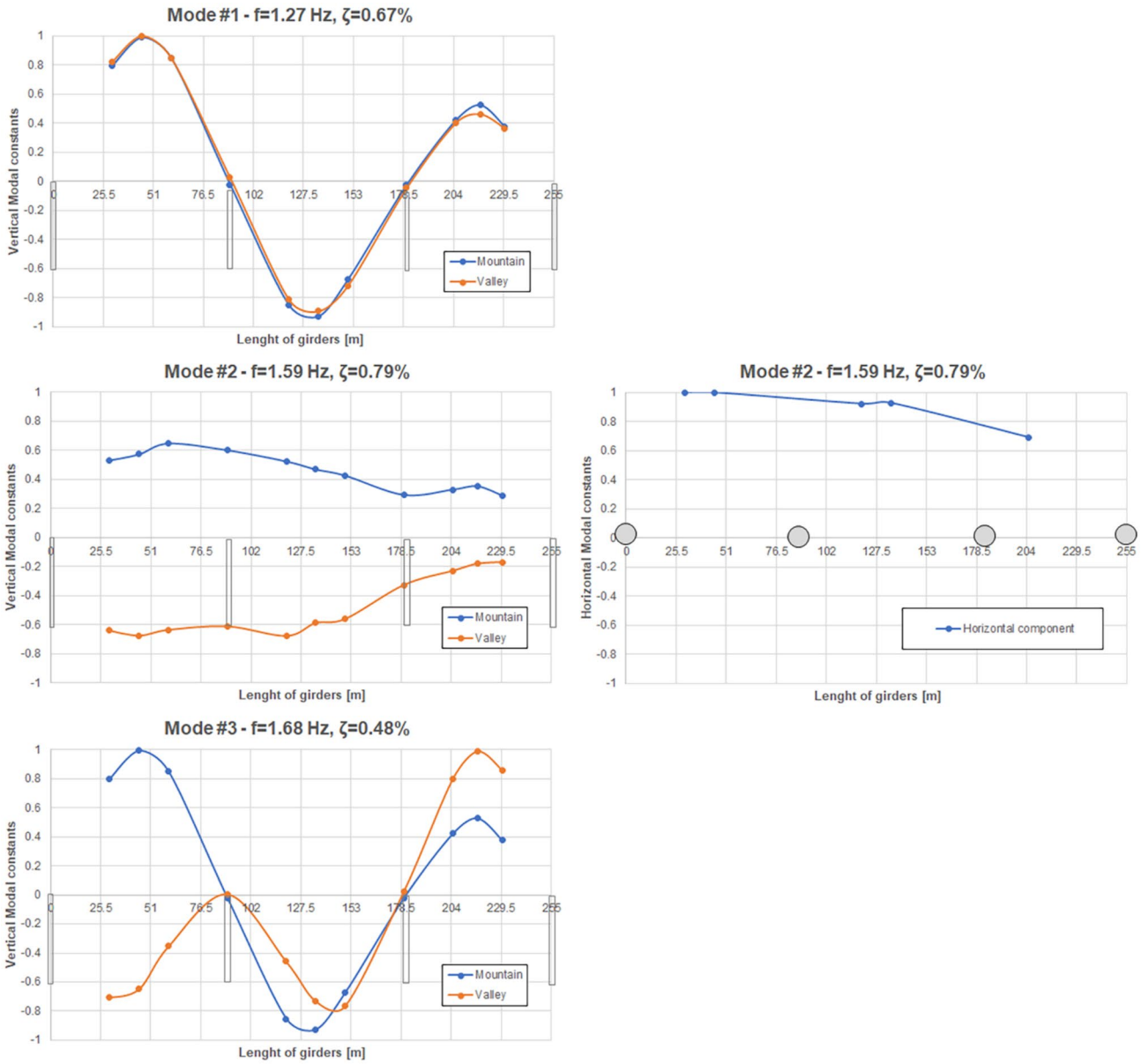

Fig. 9 Mode shapes of the three modes identified with OMA. The 2nd mode has both the components in the vertical and in the horizontal directions with respect to the deck

the mountain extremity and positive in the valley extremity. Vertical oscillations were dominant in lower modes, and deck vibrates according to shapes of a multi-span continuous beam.

Also with EMA, Mode 2 (1.57 Hz, $\zeta = 1.06\%$) vibrated both in out-of-plane and in-plane directions of the deck. The difference in frequency respect to OMA is about $+1.26\%$. Maximum amplitude was again recorded in the first span if we consider the extremity near to the mountain, and in the middle of the central span, if we consider the extremity near to the valley, and the oscillation amplitudes of homologous points located on both sides of the deck were not equal (also from an engineering point of view) as OMA but are again with opposite signs. These modes are once more reminiscent of the spatial deformation of the first bending modes of a multi-span continuous beam.

A dynamic behavior analogous to that of North carriageway was encountered in identifying the vibration modes of South carriageway, with some little differences as observed for OMA. Three frequencies and the associated mode shapes were always identified. The most important differences are that all the modes still involve the deformation of the whole deck, with a prevalence of an in-phase oscillation of the two extremities of the deck

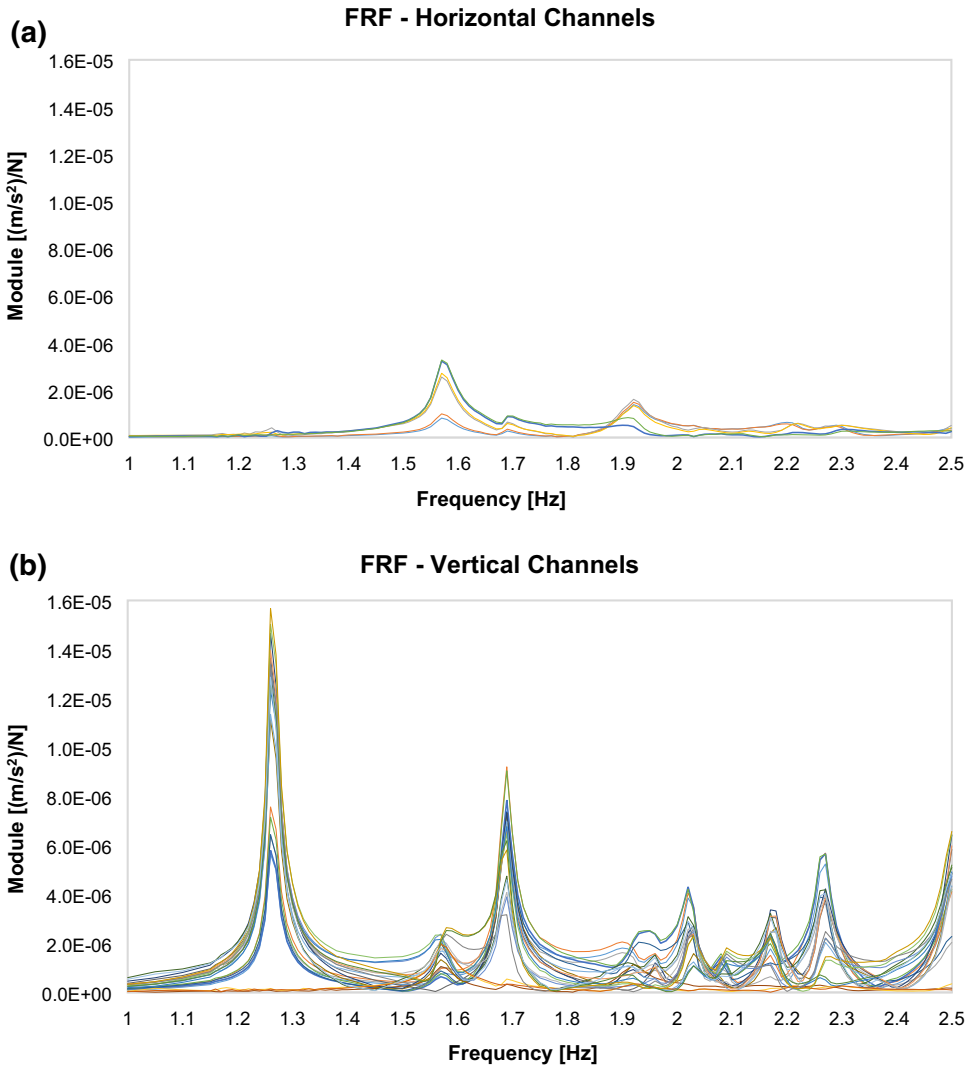

Fig. 10 FRF of horizontal (**a**) and vertical channels (**b**) for the EMA on the North carriageway [21]

in the vertical plane but with very big different values in the two extremities. These modes have very close natural frequency values as just observed in OMA, respectively, 2.05 Hz and 2.11 Hz for Mode 1 and Mode 2. The third mode corresponds to the natural frequency value equal to 2.20 Hz and presents a modal with different signs near the piers P6 and P7 in the two extremities of mountain and valley.

The EMA on the northern carriageway, in which the central spans were instrumented, allowed the identification of the first three modes, which present components of high amplitude on those spans and almost equal to zero on the shore spans. For this reason, for EMAs even in the presence of greater input energy, it is not sufficient to generate appreciable modal amplitudes for the first three modes in the shoulder spans. The EMA tests on the southern carriageway allowed the identification of higher modes, as also observed in OMA, whose contributions in terms of amplitude of vibration on the side bays are more significant.

The damping derived from the processing of EMA is compatible with the real dissipative capacity of the structure in the field of small vibrations.

5 Comparison with FEM

In Table 4, a comparison between the results of all the experimental tests and those derived from the numerical model is reported in terms of frequencies of the identified modes.

From the observation of the results, we can deduce an excellent agreement both between the results provided by the different experimental tests (OMA and EMA), and between them and the estimates of the numerical model.

In particular, the percentage error on the frequencies identified by OMA and EMA and the numerical model is contained within about 6.5%, both for the North (first three modes) and for the South (higher modes) carriageways. The modal forms experimentally identified in

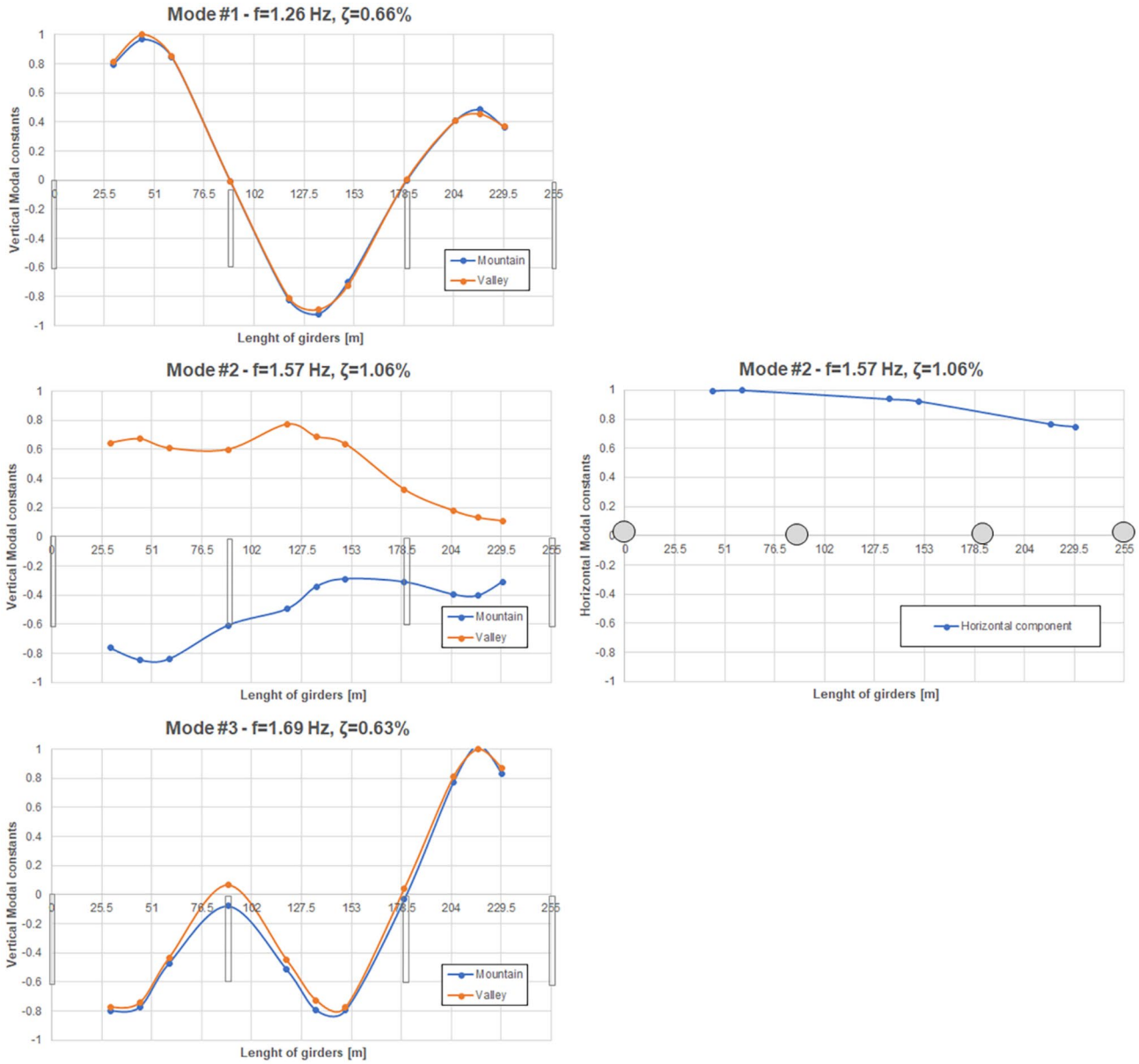

Fig. 11 Mode shapes of the three modes identified with EMA. The 2nd mode has both the components in the vertical and in the horizontal directions with respect to the deck

Table 4 Comparison between numerical and experimental frequencies of the identified modes

Frequency (Hz)	FEM (Hz)	OMA north (Hz)	EMA north (Hz)	OMA south (Hz)	EMA south (Hz)
f1	1.23	1.27	1.26	–	–
f2	1.67	1.59	1.57	–	–
f3	1.64	1.68	1.69	–	–
f4	1.99	–	–	2.06	2.05
f5	2.03	–	–	2.11	2.11
f6	2.10	–	–	2.21	2.2

correspondence with the natural frequencies also show good agreement with the values taken from the numerical model in the positions of the measurement sensors; this allows us to confirm the identification of three modes and allows a complete experimental validation of the numerical model. The contained local variations found in the values of the modal constants identified by OMA and EMA are due to the normal dispersion of the measured data; in particular, the position of the vertical maximum in the first two modes, which in the OMA identification appears in span 2, in the EMA identification, in accordance with the numerical model, occurs instead in span 3. In this case, the

forcing, therefore, allows a more precise identification of the modal form.

In conclusion, it is necessary to outline the fact that the identification carried out refers to an operating configuration in which the isolators are similar to constraints with known elastic characteristics and there is no involvement of piers. Differently, with an earthquake, the isolators would modify damping and modal masses participating for each mode.

6 Conclusions

This research dealt with an application of dynamic methods for structural identification of the Adda viaduct, inside the roadway between Milan and Brescia (North Italy). The viaduct is composed of two side-by-side decks each made up of 20 spans with different lengths, supported on circular piers by means of elastomeric seismic isolators. Before opening, the viaduct was subjected to static and dynamic tests, the latter with environmental and forced excitation of known value.

The vertical deflections were measured by means of an optical measurement and LVDT systems before, during, and after the trucks were positioned on the bridge deck on both the carriageways. All the results are lower than the expected ones obtained in design, and the deflections were almost completely reversible after complete unloading. As for the "long-term loading" case, the agreement is generally very good. The influence of solar radiation on the deformability of the deck was likewise investigated and clearly understood.

Natural frequencies, modes shapes and damping factors of the first modes of the viaduct were estimated on the basis of a series of AVTs and HFTs. In general, the two approaches, very different from each other due to the unknown of the input in the AVTs, give the same results with very little differences which are completely marginal from an engineering point of view. In the North carriageway, in particular, it was possible to identify the first three modes below 2 Hz because the spans, being central, allow recording even small environmental noises that excite the lower frequencies. In the south carriageway, it was not possible to identify the first natural modes either with the AVT or with the HFT, due to the presence of the bridge abutments which strongly condition the dynamic response.

In all the various identifications, the main modes are associated with modal shapes that deform the deck in the out-of-plane directions. The components of the modal shapes of the deck are always low, except for the second identified mode in both carriageways.

Finally, it is possible to affirm that the dynamic characterization of Adda viaduct provides important advice to bridge constructors with respect to the use of both static and dynamic data to assess the quality of the adopted technique for the realization of the viaducts. Furthermore, these experimental results permit a clear interpretation of future long-term monitoring data on the Adda Viaduct.

Acknowledgements The authors wish to gratefully acknowledge the "Società di Progetto Brebemi S.p.A." for the permission to use the static and dynamic testing data of the Brebemi Viaducts.

Compliance with Ethical Standards

Conflict of interest The authors declare that they have no conflict of interest.

References

1. Del Grosso AE (2014) Structural health monitoring standards. IABSE Symp Rep 102:2991–2998. https://doi.org/10.2749/222137814814069804
2. Gatti M (2019) Structural health monitoring of an operational bridge: a case study. Eng Struct 195:200–209. https://doi.org/10.1016/j.engstruct.2019.05.102
3. Mufti AA (2002) Structural health monitoring of innovative canadian civil engineering structures. Struct Heal Monit An Int J 1:89–103. https://doi.org/10.1177/147592170200100106
4. Aktan AE, Catbas FN, Grimmelsman KA, Pervizpour M (2002) Development of a model health monitoring guide for major bridges. Rep. Dev. FHWA Res. Dev. Available at: https://www.scribd.com/document/343127708/Development-of-a-Model-Health-Monitoring-Guide-for-Major-Bridges
5. Bergmeister K (2002) Monitoring and safety evaluation of existing concrete structures: state-of-the-art report (Fib Task Group 5.1). International Federation for Structural Concrete
6. ISO (International Organization for Standardization) (2003) Mechanical vibration and shock—guidelines for dynamic tests and investigations on bridges and viaducts. ISO 14963:2003
7. Rucker W, Hille F, Rohrmann R (2006) Guideline for structural health monitoring. Final report, Structural Assessment, Monitoring and Control. SAMCO, Berlin
8. National standard of the Russian Federation (2010) GOST R 53778:2010. Building and Structures. Technical Inspections and Monitoring Regulations [in English]
9. Österreichisches Forschungsgellschaft RVS (2012) Quality assurance for structural maintenance, surveillance, checking and assessment of bridges and tunnels, monitoring of bridges and other engineering structures [in German]
10. Moreu F, Li X, Li S, Zhang D (2018) Technical specifications of structural health monitoring for highway bridges: new Chinese structural health monitoring code. Front Built Environ. https://doi.org/10.3389/fbuil.2018.00010
11. Fujino Y, Siringoringo DM (2008) Structural health monitoring of bridges in Japan: an overview of the current trend. In: Fourth International Conference on FRP Composites in Civil Engineering (CICE2008), 22–24 July 2008, Zurich, Switzerland
12. Fujino Y, Kawai Y (2016) Technical developments in structural engineering with emphasis on steel bridges in Japan. J JSCE 4:211–226. https://doi.org/10.2208/journalofjsce.4.1_211
13. D.M. 17/01/2018 - Ministero delle Infrastrutture e dei Trasporti (2018) Aggiornamento delle "Norme Tecniche per le Costruzioni", pp. 1–198 (in Italian)
14. UNI Standard UNI (Ente nazionale italiano di unificazione). Vibrations on bridges and viaducts—guidelines for the execution of dynamic tests and surveys, Italy

15. Benedettini F, Dilena M, Morassi A (2015) Vibration analysis and structural identification of a curved multi-span viaduct. Mech Syst Signal Process 54–55:84–107. https://doi.org/10.1016/j.ymssp.2014.08.008
16. Lamonaca F, Scuro C, Grimaldi D et al (2019) A layered IoT-based architecture for a distributed structural health monitoring system. ACTA IMEKO 8:45. https://doi.org/10.21014/acta_imeko.v8i2.640
17. Lamonaca F, Sciammarella PF, Scuro C et al (2018) Internet of things for structural health monitoring. In: 2018 Workshop on metrology for industry 4.0 and IoT. IEEE, pp 95–100. https://doi.org/10.1109/METROI4.2018.8439038
18. Lamonaca F, Sciammarella PF, Scuro C et al (2018) Synchronization of IoT layers for structural health monitoring. In: 2018 Workshop on metrology for industry 4.0 and IoT. IEEE, pp 89–94. https://doi.org/10.1109/METROI4.2018.8428329
19. Scuro C, Sciammarella PF, Lamonaca F et al (2018) IoT for structural health monitoring. IEEE Instrum Meas Mag 21(6):4–14. https://doi.org/10.1109/MIM.2018.8573586
20. Consorzio BBM (2014) Collegamento autostradale di connessione tra le città di Brescia e Milano. CUP E3 1 B05000390007. Esecuzione lavori. Corpo autostradale. Opere d'arte maggiori. Lotto 7–VI003. VIADOTTO ADDA–Km 43 + 220,95 – 44 + 487,92. Rap. prova di carico statica (in Italian)
21. Consorzio BBM (2014) Collegamento autostradale di connessione tra le città di Brescia e Milano. CUP E3 1 B05000390007. Esecuzione lavori. Corpo autostradale. Opere d'arte maggiori. Lotto 7–VI003. VIADOTTO ADDA–Km 43 + 220,95 – 44 + 487,92. Rap. prova di carico dinamica (In italian)
22. Peeters B, Van der Auweraer H, Guillaume P, Leuridan J (2004) The PolyMAX frequency-domain method: a new standard for modal parameter estimation? Shock Vib 11:395–409. https://doi.org/10.1155/2004/523692